

Los Alamos National Laboratory is operated by the University of California for the United States Department of Energy under contract W-7405-ENG-36.

TITLE: OPTIMIZING LINER IMPLOSIONS FOR HIGH ENERGY DENSITY PHYSICS EXPERIMENTS

AUTHOR(S): Carl Ekdahl, Los Alamos National Laboratory
Stanley Humphries, Jr., University of New Mexico

RECEIVED
JAN 21 1997
OSTI

SUBMITTED TO: Megagauss VII Proceedings

DISTRIBUTION OF THIS DOCUMENT IS UNLIMITED

MASTER

By acceptance of this article, the publisher recognizes that the U.S. Government retains a nonexclusive, royalty-free license to publish or reproduce the published form of this contribution, or to allow others to do so, for U.S. Government purposes.

The Los Alamos National Laboratory requests that the publisher identify this article as work performed under the auspices of the U.S. Department of Energy.

Los Alamos Los Alamos National Laboratory
Los Alamos, New Mexico 87545

DISCLAIMER

Portions of this document may be illegible in electronic image products. Images are produced from the best available original document.

DISCLAIMER

This report was prepared as an account of work sponsored by an agency of the United States Government. Neither the United States Government nor any agency thereof, nor any of their employees, make any warranty, express or implied, or assumes any legal liability or responsibility for the accuracy, completeness, or usefulness of any information, apparatus, product, or process disclosed, or represents that its use would not infringe privately owned rights. Reference herein to any specific commercial product, process, or service by trade name, trademark, manufacturer, or otherwise does not necessarily constitute or imply its endorsement, recommendation, or favoring by the United States Government or any agency thereof. The views and opinions of authors expressed herein do not necessarily state or reflect those of the United States Government or any agency thereof.

OPTIMIZING LINER IMPLOSIONS FOR HIGH ENERGY DENSITY PHYSICS EXPERIMENTS

Carl Ekdahl, and Stanley Humphries, Jr.¹

Los Alamos National Laboratory, Los Alamos, USA

¹ University of New Mexico, Albuquerque, USA

Introduction

Cylindrical metal shells imploded by magnetic fields - liners - are used as kinetic energy drivers for high energy density physics experiments in hydrodynamics and dynamic material property measurements. There are at least three ways in which liners have been, or are expected to be, used to produce high energy density, i.e., high pressure, in target materials. A common approach uses the liner as a convergent flyer plate, which impacts a material target cylinder after having been shocklessly accelerated across an intervening gap. The resultant shock and piston hydrodynamic flow in the target are used in exploration of a wide variety of phenomena and material properties. Another common method is to slowly compress a liner containing a material sample in a such fashion that little heating occurs. This technique is most useful for investigated physical properties at low temperature and extreme density. Finally, one can use a hybrid approach to shock heat with an impacting liner followed by slower adiabatic, if not isentropic, compression to explore material properties in extrema. The magnetic fields for driving these liners may be produced by either high explosive pulsed power generators or by capacitor banks. Here we will consider only capacitor banks.

The common objective of these approaches is the generation of high pressure in the target, although each method has different criteria to consider in optimizing experimental design for the highest possible pressure. In this paper we will focus on optimizing the technique of using a liner as a convergent flyer plate to produce a high shock pressure. Other considerations are the experimental target size, and the available duration of unperturbed material flow. These are coupled, of course, and are motivated by considerations of experiment scale and diagnostics. Much of the work presented here was motivated by considerations in the design of the Atlas 36-MJ hydrodynamic experimentation facility.

The highest impact velocity of the inner surface of the liner with the target will produce the highest shock pressure in the experiment. This can be seen from the shock Hugoniot equation of state formulated in terms of the shock and particle velocities ¹. For almost all materials of interest this can be written as $v_s = c + s u_p$. The shock pressure is given by $p = \rho u_p v_s$. For the case of a liner impacting a target with velocity v one equates pressure in the flyer and target $\rho_T(c_T + s_T u_p)u_p = \rho_L[c_L + s_L(v - u_p)](v - u_p)$, and solves for $u_p(v)$, and then $p(v)$. Clearly, the pressure is only a function of liner velocity at impact and material parameters. Thus, optimizing for highest velocity at impact will ensure highest pressure for a given selection of materials. To simplify the

problem, we focus on the case of liner and target made from the same material, in which case the pressure is $p = \rho \frac{v}{2} (c + s \frac{v}{2})$.

Liner and Capacitor Bank Models

We began our study using a simple, analytic model, in which the liner is driven by currents flowing on its surface, and diffusion of the magnetic field into the metal is ignored. This model was first developed by J. Parker to design liners for the Pegasus capacitor bank at Los Alamos². After this model was used to initially narrow down the range of design parameters, we used 1-D Lagrangian, fully MHD calculations to refine the final results.

We first consider an incompressible liner with outer radius r_2 , inner radius r_1 , mass m , and height h , imploded by a current I on its surface. Incompressibility and mass conservation demand that the cross-sectional area, $A = \pi(r_2^2 - r_1^2)$, remains constant. Differentiation of the area shows that the inner surface always implodes with a higher velocity than the outer, $v_1 = r_2 v_2 / r_1$, suggesting thick, high convergence liners that take advantage of this mechanical amplification to achieve the high velocities needed to generate high pressure in the target.

The equation of motion of the inner surface for the liner is

$$\frac{dv_1}{dt} = -\frac{v_1^2}{r_1} - \frac{1}{\ln\left(\frac{r_2}{r_1}\right)} \left[\frac{\mu_0 I^2}{8\pi^2 \rho r_1 r_2^2} - \frac{v_1^2}{2r_1 r_2^2} (r_2^2 - r_1^2) \right]. \quad (1)$$

In the limit of thin liners and low convergence implosions this reduces to the familiar thin liner or "slug" model equation of motion,

$$\frac{d^2 r}{dt^2} = -\frac{\mu_0 h}{4\pi} \frac{I^2}{mr}, \quad (2)$$

where r is the mean radius. The condition for validity of Eq. 2 is that $\chi^2 \delta \ll 1$, where $\chi = R/r$ is the convergence, and $\delta = \Delta/R$ is the thickness ratio. Here R is the mean initial radius, and Δ is the initial thickness. The importance of high current drive is clear from Eq. 2, especially given constraints placed on the minimum mass allowable. Because thick liners and high convergence are a means to the highest possible pressures, the condition for validity of Eq. 2 is violated, and we used Eq. 1 instead. The system of equations formed from Eq. 1 and the circuit model of the capacitor bank were integrated with a fourth order Runge-Kutta algorithm.

After a survey using the analytic model, the optimum liner parameters were refined using the Crunch 1-D Lagrangian MHD code³. Crunch uses the Los Alamos Sesame tables⁴ for equation of state data. The material conductivity model for Crunch uses experimental data⁵ below 2×10^4 K interpolated to theoretical values⁶ above 1×10^5 K. A two loop circuit model that includes the possibility of time varying elements is coupled to the 1-D hydrodynamics of the liner implosion in Crunch calculations.

For analytic scaling, the bank was modeled as a simple LRC circuit:

$$\frac{d^2 Q}{dt^2} + \frac{R}{L} \frac{dQ}{dt} + \frac{1}{LC} Q + \frac{d}{dt} \left(\frac{L_t}{L} \frac{dQ}{dt} \right) = 0, \quad (3)$$

where Q is the charge on the capacitors, and the time varying inductance of the liner is

$$L_t(t) = \frac{\mu_0 h}{2\pi} \ln \left(\frac{r_2(0)}{r_2(t)} \right). \quad (4)$$

In this model the total fixed inductance L includes bank, transmission line, and header inductances up to the initial position of the liner. The resistance R includes the small, but time varying, liner resistance. The Atlas design incorporates a small shunt resistance for damping high-frequency ringing, which was ignored in the analytic model, but was included in the 1-D Crunch calculations. To illustrate the effect of capacitor bank design on liner performance we will use the 36-MJ Atlas capacitor bank under construction at Los Alamos as an example. Atlas will have 600 capacitors, and it was initially conceived that they would be arranged in a 600-kV Marx configuration. There is a detailed conceptual electrical design for this configuration. However, with fixed energy, rearranging the capacitors in a lower impedance, lower voltage configuration would increase the drive current and implosion force on the liner as clearly seen from Eq. 2.

To explore the effect of lower voltage configurations we considered variations of the 600-kV concept design. In all cases the series resistance, R , was adjusted to limit voltage reversal on the capacitors to 15% when discharged into a dead short. We varied the bank inductance and capacitance by recalling that the frequency $\omega = 1/\sqrt{L_B C}$ remains constant for any configuration provided the number of capacitors is unchanged. The transmission line inductance was varied by reducing its thickness, hence inductance, in direct proportion to charge voltage. Scaling of the 36-MJ Atlas design parameters is shown in table 1.

Scaling Constant κ	Charge Voltage V_b (kV)	Bank Cap. C_b (μF)	Bank Ind. L_b (nH)	Series Damping Res. R_b (m Ω)	X-Line Ind. L_x (nH)	Shunt Damping Res. $R_{ }$ (m Ω)	Header Ind. L_h (nH)	Total Ind. L (nH)
1	600	200	9	12	6	80	10	25
0.8	480	312.5	5.76	8	4.8	64	8	18.56
0.6	360	555.6	3.24	5	3.6	48	6	12.84
0.4	240	1250	1.44	3	2.4	32	4	7.84
0.2	120	5000	0.36	0.86	1.2	16	2	3.56
Scaling:	κV_{b0}	C_{b0}/κ^2	$\kappa^2 L_{b0}$	$2\gamma L_{\Sigma 0}$	κL_{x0}	$\kappa R_{ 0}$	κL_{h0}	ΣL_{i0}

Table 1. Atlas bank design parameter variations for analytic and 1-D liner calculations

To complete the model one assumes that the Joule heating of the liner material is distributed uniformly throughout its volume. Admittedly this is inconsistent with the initial

assumption of surface current, but has little effect on results. We follow Tucker and Toth in postulating that the resistivity of the liner material is approximately only a function of the specific electrical action⁷

$$G(t) = \int_0^t j^2(\tau) d\tau, \quad (5)$$

where j is the current density. Using this model Parker found that aluminum was the material that resulted in highest liner velocities without completely melting. So we use aluminum in all of the calculations presented here. This to retain maximum solid material strength at high velocities in order to suppress the growth of MHD instability.

Figures 1 and 2 show the radii and velocities of the inner and outer surface of an aluminum liner imploded by the 240-kV Atlas model to impact a target with a radius of 0.5 cm as calculated using this simple model. The action calculated from Eq. 4 is just sufficient to begin melting at impact with the target with a final velocity of 2.6 cm/ μ s. (Note that much of the final velocity in this incompressible model results from simple mechanical multiplication.) This liner would produce an 8-Mbar shock pressure in the aluminum target.

Stability Considerations

Liner performance can be seriously limited by MHD instability. The outer boundary of the liner is always MHD unstable. The dangerous modes are short-wavelength axial (azimuthal modes are stabilized by magnetic field line tension⁸). In analogy to the Rayleigh-Taylor instability, the magnetic field plays the role of a light fluid pushing on the metal, which eventually loses strength through Joule heating. Indeed, there may even be experimental evidence for an MHD analogue to the Richtmyer-Meshkov instability when the shock generated on target impact reaches the outer surface of the liner, which is a diffuse boundary between metal and the light magnetic "fluid".

During acceleration the growth of the MHD instability may limit the distance through which the liner implodes before it is disrupted. The instability grows rapidly in the outer part of the liner, where the metal has lost strength through melting by Joule heating. Only instability growth slower than mechanical thickening of the liner will prevent break through. Moreover, breakthrough may be inhibited if a large part of the inner region of the liner remains unmelted, retaining some strength.

The initial exponential growth of the instability can be estimated from the theory of stability of a plasma column⁹, which reduces to the familiar Rayleigh-Taylor growth rate driven by a massless magnetic fluid for axial modes with wavelength much shorter than the radius of the liner. The extensive historical work on plasma pinches also shows a possible path to stabilization of this dangerous MHD mode by imbedding an axial, stabilizing magnetic field.

Following initial exponential growth the instability saturates through coalescence to a slower, nonlinear growth to give an agitated region width¹⁰

$$\eta(t) = \alpha \left[\int_0^t \sqrt{g(\tau)} d\tau \right]^2, \quad (6)$$

where $g(t)$ is the interface acceleration. From Eq. 6 it can be easily shown that the nonlinear amplitude $\eta(t)$ is proportional to the distance the liner moves if the acceleration is a power law; $g(t) \propto t^k$, where $k \geq 0$. The growth factor, α , is about 0.05 for pure hydro with fluid interfaces¹¹, but can be ten times that for MHD in fully ionized plasmas¹². The amplitude at which the instability transitions from exponential growth is wavelength dependent¹³, $\eta_0 \approx \lambda / 10$, making long wavelength initial perturbations quite risky. This imposes serious demands on liner fabrication.

To illustrate the danger of the MHD instability the nonlinear amplitude is compared with the liner thickness for the example in Fig. 1 and 2. For this comparison, shown in Fig. 3, the instability was assumed to transition to nonlinear growth at 1.0 μs , and then grow with a modest $\alpha=0.1$. From Fig. 3 it is seen that the instability would have broken through a fluid liner at about 4.5 ms; long before impact with the target. Therefore, we strive to reduce through material strength by keeping the liner solid, insofar as possible. Thus, we placed strict limits on liner heating in our study. That is, we limited liner heating to ensure that a significant fraction of the liner would be solid. For example, in the simple analytic model calculations we restricted solutions to those with a final electrical action that would only begin to melt the liner. And, in the 1-D modeling we restricted solutions to those retaining a solid thickness equal to the target radius at time of impact.

Optimization

The procedure used to find the optimum liner parameters for maximum target pressure was straightforward. For each 36-MJ bank configuration, the liner initial parameters that would produce the maximum velocity (hence, pressure) was found by surveying the initial mass and radius using the analytic model. For example, Fig. 4 shows the impact velocity achieved on the 600 kV variation by a 40-gm liner as a function of the initial radius. From this one reads that the highest velocity achievable with a 40-gm liner is 15 mm/ μs using a 2.4 cm initial radius. A family of such curves was generated for different mass liners, shown in Fig. 5. This clearly shows that the maximum velocity continues to increase without bound as the mass is reduced. But, when one restricts the solutions to those in which the liner remains unmelted, there appears a unique solution in mass and initial radius that gives the absolute maximum impact velocity for the 600-kV bank configuration. This is the optimum liner design for 600 kV. As seen from Fig. 6, this design is a 30-gm liner with an initial radius of 2.1 cm, which impacts the target with a velocity of 18 mm/ μs .

This procedure was repeated for each of the bank options in listed in Table 1, and the results are shown in Fig.7. So, for each bank voltage a unique optimum liner design was found. The final velocities calculated for each optimum design are presented in Fig. 8.

The next step in our study was to use these optima as initial starting points for refinement using the 1-D Lagrangian code. Having these preliminary results as initial parameters greatly reduced the amount of time required to complete the 1-D calculations and optimization, which proceeded roughly along the same path outlined above. One difference was that the 1-D calculations gave a detailed picture of the variation of Joule heating through the liner resulting from current diffusion from the outside, so solutions could be restricted to those that retained 0.5 cm of solid metal at

impact to suppress instability growth and provide an adequate duration of high pressure in the target.

The results of the 1-D optimization are shown in Fig. 9. The lower impact velocities calculated in 1-D are attributed to use of real EOS data leading to compressibility of the material, because a significant fraction of the final velocity in the analytic model results from mechanical multiplication; a feature of incompressibility. Finally, we show the calculated shock pressure in the target and its duration, which represents the window for hydrodynamic experiments. Clearly, the lower voltage bank options present an advantage for hydrodynamic experiments. These, and similar, calculations were the basis of the decision to configure Atlas in a 36-MJ, 240-kV design.

¹ J. D. Johnson, "General Features of Hugoniot", *Los Alamos National Laboratory Report LA-UR-95-3555*, 1995

² J. Parker, "A Primer on Liner Implosions with Particular Application to the Pegasus II Capacitor Bank", *Los Alamos National Laboratory Athena Program Report*, Oct. 1993

³ Stanley Humphries, Jr. and Carl Ekdahl, "Numerical Models of Pressure Pulse Generation by Imploding Metal Liners", *IEEE Trans. Plasma. Sci.*, Dec. 1996

⁴ G. K. Straub and W. A. Harrison, *Phys. Rev. B* **31**, 1985, p. 6155

⁵ T. J. Tucker and R. P. Toth, "EBWI: A Computer Code for the Prediction of the Behavior of Electrical Circuits Containing Exploding Wire Elements", *Sandia National Laboratory Report SAND-75-0041*, 1975

⁶ G. A. Rinker, "Systematic Calculations of Plasma Transport Coefficients for the Periodic Table", *Phys. Rev. A* **37**, 1988, p. 1284

⁷ T. J. Tucker and R. P. Toth, "EBWI: A Computer Code for the Prediction of the Behavior of Electrical Circuits Containing Exploding Wire Elements", *Sandia National Laboratory Report SAND-75-0041*, 1975

⁸ S. Chandrasekhar, *Hydrodynamic and Hydromagnetic Stability*, N. Y. Dover 1981, p. 466

⁹ M. Kruskal and J. L. Tuck, "The Instability of a Pinched Fluid with a Longitudinal Magnetic Field", *Proc. Roy. Soc. A*, 1957, p. 222-237

¹⁰ D. Shvarts, U. Alon, D. Ofer, R. L. McCrory, and C. P. Verdon, "Nonlinear Evolution of Multimode Rayleigh-Taylor Instability in Two and Three Dimensions", *Phys. Plasmas* **2**, 1995, p.2465-2472

¹¹ D. L. Youngs, "Numerical Simulation of Turbulent Mixing by Rayleigh-Taylor Instability", *Physica D* **12**, 1984, p.32-44

¹² D. L. Peterson, R. L. Bowers, J. H. Brownell, A. E. Greene, K. D. McLenithan, T. A. Oliphant, N. F. Broderick, and A. J. Scannapieco, "Two-Dimensional Modeling of Magnetically Driven Rayleigh-Taylor Instabilities in Cylindrical Z-Pinches", *Phys. Plasmas* **3**, 1996, p.368-381

¹³ N. M. Hoffman, "Hydrodynamic Instabilities in Inertial Confinement Fusion", in: *Laser Plasma Interaction 5: Inertial Confinement Fusion*, (Ed. M. B. Hooper), Bristol: Inst. Phys. Publishing, 1995, p.105-137

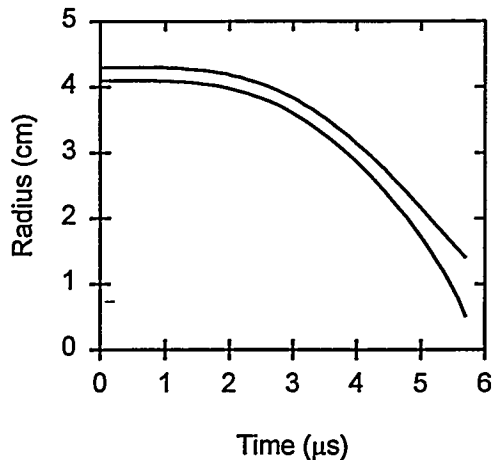


Fig. 1 Inner and outer radii of liner imploded with 240-kV bank configuration

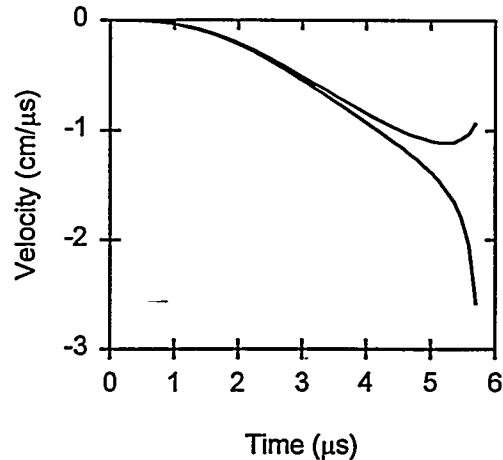


Fig. 2 Inner and outer surface velocities for 240 kV bank

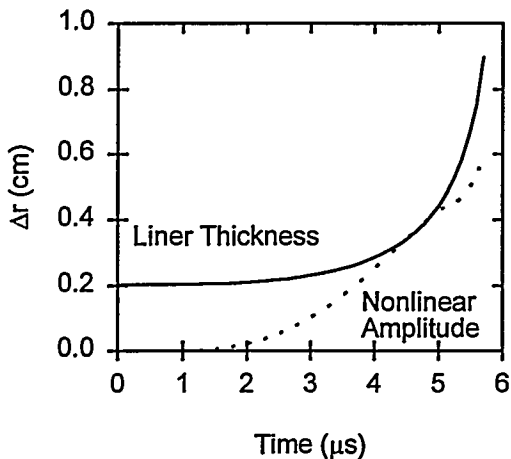


Fig. 3 Nonlinear growth of MHD instability compared with liner thickness

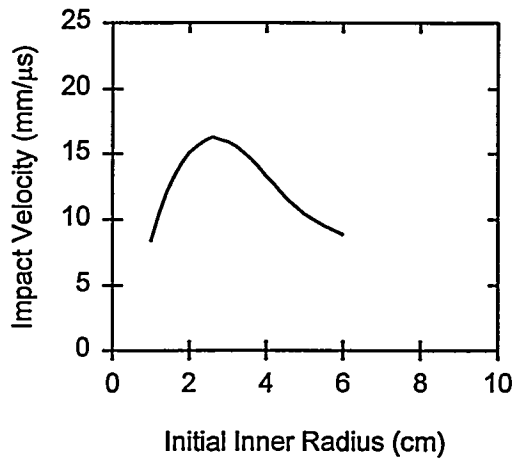


Fig. 4 Impact velocity of 40 gm liner imploded with 600 kV bank

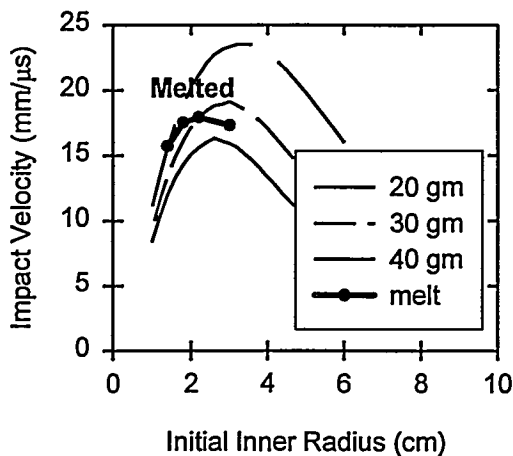


Fig. 5 Impact velocities of liners with varying mass showing unmelted liner limit

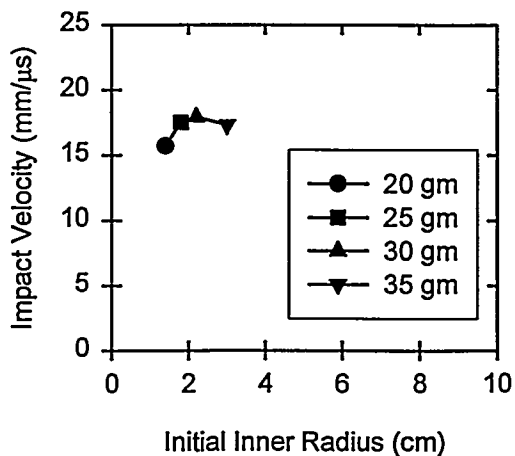


Fig. 6 Maximum velocity of unmelted liners imploded by 600 kV bank

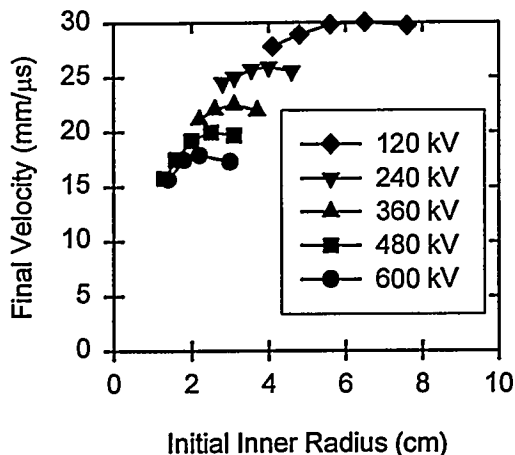


Fig. 7 Melt limited liner impact velocities for different bank configurations

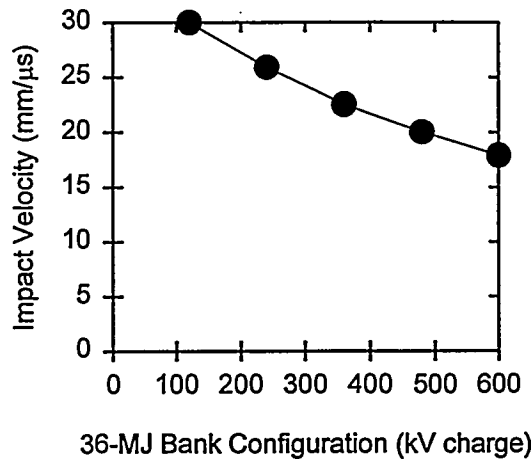


Fig. 8 Maximum liner impact velocities calculated from analytic model

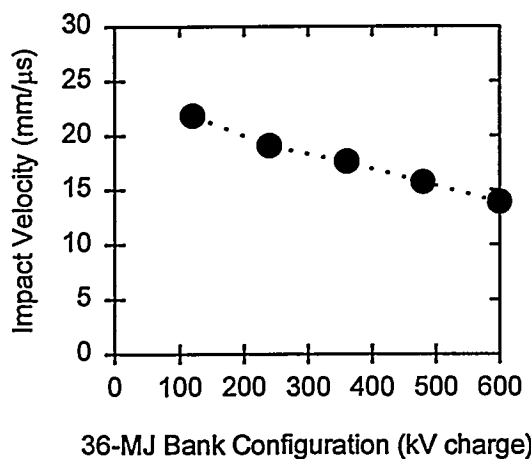


Fig. 9 Maximum liner impact velocities calculated from 1-D Lagrangian code

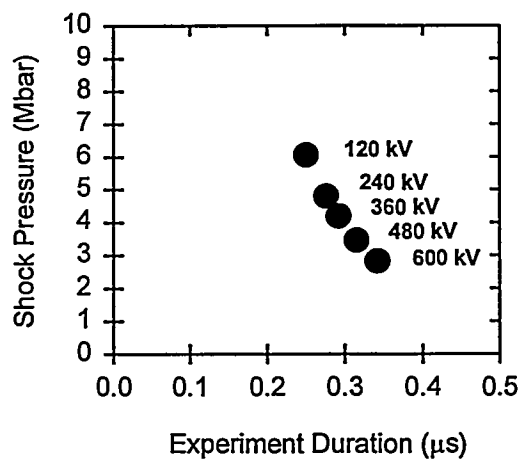


Fig. 10 Maximum shock pressure in target and its duration calculated from 1-D Lagrangian hydro code.